# Heterometallic titanium-organic frameworks by metal-induced dynamic topological transformations

Natalia M. Padial,[†,⊥,#,*] Belén Lerma-Berlanga,[†, #] Neyvis Almora-Barrios,[†] Javier Castells-Gil,[†] Iván da Silva,[§] María de la Mata,[◊] Sergio I. Molina,[◊] Jesús Hernández-Saz,[‡] Ana E. Platero-Prats,[¬,¤] Sergio Tatay,[†] Carlos Martí-Gastaldo[†,*]

[†] Functional Inorganic Materials Team, Instituto de Ciencia Molecular (ICMol), Universitat de València, Paterna 46980, València, Spain.

[§] ISIS Facility, Rutherford Appleton Laboratory, Chilton, Didcot, Oxfordshire, OX11 0QX, United Kingdom.

[◊] Departamento de Ciencia de los Materiales e I.M. y Q.I., Facultad de Ciencias, IMEYMAT, Universidad de Cádiz, Campus Río San Pedro, s/n, 11510, Cádiz, Spain.

[‡] Departamento de Ingeniería y Ciencia de los Materiales y del Transporte, Escuela Politécnica Superior, Universidad de Sevilla, 41011, Sevilla, Spain.

[¬] Departamento de Química Inorgánica, Universidad Autónoma de Madrid, 28049, Madrid, Spain.

[¤] Condensed Matter Physics Center (IFIMAC), Universidad Autónoma de Madrid, 28049, Madrid, Spain.

**ABSTRACT:** Reticular chemistry has boosted the design of thousands of Metal and Covalent Organic Frameworks for unlimited chemical compositions, structures and sizeable porosities. The ability to generate porous materials at will based on geometrical design concepts is responsible for the rapid growth of the field and the increasing number of applications derived. Despite their promising features, the synthesis of targeted homo and heterometallic titanium-organic frameworks amenable to these principles is relentlessly limited by the high reactivity of this metal in solution that impedes the controlled assembly of titanium molecular clusters. We describe an unprecedented methodology for the synthesis of heterometallic titanium frameworks by metal-exchange reactions of MOF crystals at low temperature. The combination of hard (titanium) and soft (calcium) metals in the heterometallic nodes of MUV-10(Ca) enables controlled metal exchange in soft positions for the generation of heterometallic secondary building units (SBUs) with variable nuclearity, controlled by the metal incorporated. The structural information encoded in the newly formed SBUs drives a MOF-to-MOF conversion into bipartite nets compatible with the connectivity of the organic linker originally present in the crystal. Our simulations show that this transformation has a thermodynamic origin and is controlled by the terminations of the (111) surfaces of the crystal. Reaction of MUV-10(Ca) with first row transition metals permits producing crystals of MUV-101(Fe, Co, Ni, Zn) and MUV-102(Cu), heterometallic titanium MOFs isostructural to archetypical solids as MIL-100 and HKUST. Compared to de novo synthesis, this metal-induced topological transformation provides control over the formation of hierarchical micro/mesopore structures at different reaction times and enables the formation of heterometallic titanium MOFs not accessible under solvothermal conditions at high temperature, thus opening the door for the isolation of multiple titanium heterometallic phases in the near future.

## Introduction

Metal-Organic Frameworks (MOFs) are crystalline extended structures assembled by the linkage of inorganic polynuclear clusters, termed secondary building units (SBUs), and organic linkers. For the last 15 years, the principles of reticular chemistry have guided the design of thousands of MOFs by rationalising the combination of SBUs and organic linkers with variable extension points into predetermined topologies.[1] Reticular chemistry provides control over the design of materials at a molecular level for a rich landscape of chemical compositions, structures and sizeable porosities of direct application in gas storage,[2,3] separation[4–6] or catalysis.[7,8] The rapid growth of the MOF field has built upon two main design strategies. The first one, the isoreticular approach, is based on the reticulation of sizeable organic linkers of the same geometry and connectivity. It makes possible to control the metrics and functionality of a specific framework topology that is fixed by the structural information encoded in the inorganic SBU.[9] The second one, the SBU approach, is more general in conception as it permits to target multiple MOF topologies also amenable to isoreticular functionalization, by controlling the geometry and connection points of the two building units in the framework.[10,11] The successful translation of these geometric design principles to the

1

synthesis of binary MOFs relies on finding the experimental conditions that reproduce the structural information encoded in the two chemical building units targeted. This is not a problem for the organic linker, that will retain geometry and connectivity in solution, but predicting the formation of persistent metal-oxo clusters under crystal growth forming conditions is not straightforward. The chemistry of SBUs intrinsic to archetypical families of MOFs like [Cu$_2$(H$_2$O)$_2$(RCO$_2$)$_2$] (HKUST),[12] [Cr$_3$O(H$_2$O)$_3$(RCO$_2$)$_6$] (MIL-100, MIL-101),[13,14] [Zn$_4$O(RCO$_2$)$_6$] (MOF-5)[9] or [Zr$_6$O$_4$(OH)$_4$(RCO$_2$)$_{12}$] (UiO)[15] is well understood and central to the thousands of works related to these materials published in the last years.

With the advance of the field, the application of MOFs has stressed their limitations calling for enhanced thermal, mechanical or hydrolytical stabilities and increasing levels of complexity.[16,17] The chemistry of the SBU can be used to improve the thermodynamic stability and tune the chemical reactivity of MOFs. For instance, inorganic clusters based on tetravalent metals like Ti, Zr, Hf(IV) are less prone to hydrolysis due to strong M-O bonds. Compared to these metals, titanium is less toxic, more abundant and redox active. Still, the synthesis of pre-designed titanium frameworks from targeted SBUs remains very challenging due to the high reactivity of Ti salts, which generally lead to ill-defined amorphous phases in solvothermal conditions. On the other hand, complexity at the SBU can be achieved by the combination of two or more metals in heterometallic clusters for mixed-metal MOFs that can outperform their monometallic counterparts in different applications like gas storage, separation or heterogeneous catalysis.[18,19] The intrinsic properties of Ti-MOFs make this possibility even more appealing as high-stability might be combined with tailorable electronic structure, photoactivity or chemical reactivity. However, the limitations to the chemistry of titanium are even more restrictive in this case and there is no straightforward route for their synthesis. The success of one-step synthesis relies on the use of metal ions with similar charge and ionic radii. The high polarizing power of Ti$^{+4}$ prevents direct reaction with other metals that would likely result in poor control over their distribution in the final material for the formation of segregated phases. In turn, incorporation of other metals to Ti-MOFs by post-synthetic exchange would be inadequate due to the high stability of Ti-O coordination bonds whereas the incorporation of Ti$^{+4}$ to pre-formed materials would not allow for complete metal replacement and lacks control over the positioning of titanium atoms in the structure,[20] which can result in spurious deposition of metal oxide coatings.[21]

We report an unprecedented methodology for the synthesis of heterometallic titanium-frameworks amenable to the principles of reticular chemistry. Instead of relying in the serendipitous discovery of mixed-metal clusters by trial and error, we use MOF crystals to direct the formation of SBUs with variable connection points by transmetalation reactions at low temperature. The combination of hard and soft metals in the heterometallic nodes of MUV-10 (MUV, Materials of Universidad de Valencia) enables controlled metal exchange in soft positions whilst retaining structural integrity. The offset in the coordination geometry upon metal replacement generates a thermodynamic metastable state that evolves into the formation of SBUs of decreased nuclearity and dependent on the metal incorporated. The structural information encoded in the newly formed SBUs drives the formation of bipartite nets compatible with the connectivity of the organic linker originally present in the crystal. This metal-induced topological transformation is a dynamic phenomenon and can be controlled with time until complete transformation of the material.

## Metal-exchange reactions in heterometallic SBUs combining labile and robust coordination sites

As commented above, the *de novo* synthesis of heterometallic MOFs is restricted to metals with similar reactivity in solution that allow for concomitant reaction and avoid the formation of homometallic frameworks. Post-synthetic metal-exchange is a more versatile route that enables the incorporation of a broader range of metals for heterometallic compositions not accessible by direct synthesis. Metal exchange reactions typically involve soaking of the MOF in concentrated solutions of the metal to be incorporated. The degree of exchange (often incomplete) is kinetically and thermodynamically controlled by the stability constants of the substituting cations and the strength of the M-O bond in the cluster. This is why precedents of MOF transmetalation are mostly focused in labile SBUs more prone to hydrolysis and metal replacement.[22,23] In contrast, robust MOFs with SBUs featuring strong M(IV)-O bonds, like [Zr$_6$O$_4$(OH)$_4$(RCO$_2$)$_{12}$], are less likely to undergo metal exchange at the cluster and can suffer from uncontrolled grafting at defective positions[20] or induce the undesired formation of an oxide coating.[21] Thus far, transmetalation reactions have been exclusively focused in homometallic MOFs for either labile or robust SBUs that compromise the stability of the resulting material or limit the metal exchange rate, respectively.
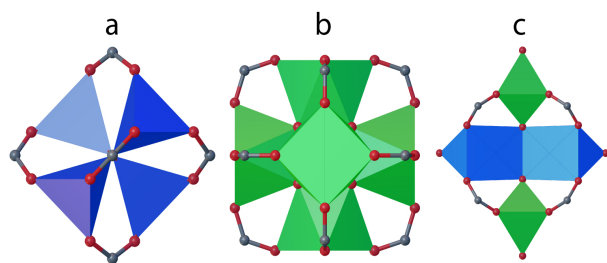


**Figure 1. Secondary-building units used in transmetalation reactions.** Structures of the metal-oxo clusters: (a) [Zn$_4$O(RCO$_2$)$_6$], Zn$_4$ (b) [Zr$_6$O$_4$(OH)$_4$(RCO$_2$)$_{12}$], Zr$_6$ and (c) [Ti$_2$Ca$_2$(O)$_2$(H$_2$O)$_4$(RCO$_2$)$_8$], Ti$_2$Ca$_2$ (this work). Blue and green metal sites stand for labile (Zn$^{2+}$) and robust (Zr$^{+4}$, Ti$^{+4}$) metal exchange positions, respectively. O, red; C, grey.

We hypothesised that these limitations might be circumvented by using heterometallic SBUs. The combination of soft (M$^{+2}$) and hard (M$^{+4}$) metals at different coordination sites in the cluster might translate into

2

quantitative metal replacement without altering the structure or jeopardizing the chemical stability of the framework.

We decided to explore this concept for the heterometallic titanium framework MUV-10(Ca).[24] This microporous solid can be synthesised at high yields from direct reaction of a calcium salt with different titanium sources. It displays a three-dimensional ***the*** topology built from the linking of eight-connected $[Ti_2Ca_2(O)_2(H_2O)_4(RCO_2)_8]$ heterometallic SBUs with btc linkers (btc = benzene-1,3,5-tricarboxylate anion). Compared to the labile and robust coordination sites in $Zn_4$ and $Zr_6$ clusters, $Ti_2Ca_2$ combines hard $Ti^{+4}$ ions in octahedral sites and capped trigonal prismatic soft $Ca^{2+}$ centres more prone to metal-exchange (**Figure 1**). Our recent work demonstrated the difficulties in producing other heterometallic solids by direct synthesis with divalent 1st row transition metal cations. In contrast to Fe, Co, Ni, Cu and Zn(II), only MUV-10(Mn) could be prepared due to the preference of Mn ions toward heptacoordinated capped trigonal prism (CTP) geometry.[24,25] We decided to investigate if same solid could be prepared by transmetalation of the calcium phase. Crystals of MUV-10(Ca) were immersed in concentrated solutions of $Mn(NO_3)_2$ in MeOH (0.2M) at 65 °C. The resulting MUV-10(CaMn) crystals were filtered and cleaned after 10 days and 30 days for further analyses. We evaluated the degree of metal exchange by inductively coupled plasma optical emission spectroscopy (ICP-OES; **Supporting Section S3.1**). The incorporation of Mn is concomitant to a decrease in Ca. Metal exchange is slightly more favourable at longer soaking times, Ca replacement increases from 11.6 % (10 days) up to 13.0 % after 30 days (**Figure 2b**, top). Compared to the postsynthetic modification of $Zn_4$ clusters in MOF-5,[26] total exchange is far from complete suggesting thermodynamic control over the transmetalation reaction.

Metal distribution was analysed with X-Ray energy dispersive spectroscopy (EDX). Mapping throughout the crystals reveals a homogeneous distribution of both metals ruling out metal clustering at the surface or the formation of segregated phases (**Supporting Section S3.2**). Scanning electron microscopy (SEM) confirms that the crystals retained the morphology and micrometric size of the starting material after metal exchange, suggesting a crystal-to-crystal reaction rather than re-crystallization in presence of the new metal (**Figure 2c**, top). Retention of the original structure was confirmed by powder X-Ray diffraction (PXRD) Le Bail refinement of the samples at variable soaking times (**Figure 2d** (top) and **Supporting Section S3.3**). The absence of additional peaks discards the formation of an additional phase upon metal-exchange. The changes in the relative intensities of the [100] reflection possibly originates from preferential orientation of the crystals as we avoided grinding to prevent amorphization. Crystals were activated by using the protocol reported for MUV-10(Ca) to analyse the effect of metal exchange over the porosity of the solid (**Supporting Section S3.4**). The $N_2$ isotherm collected confirmed that MUV-10(CaMn) retained the original porosity with an insignificant impact over the BET surface area or the experimental pore diameter. Also important, PXRD and porosity data of the crystals after soaking in concentrated HCl and NaOH(aq) solutions confirm that transmetalation does not compromise the hydrolytical stability of the parent solid that originates from the presence of robust Ti-O nodes (**Supporting Section S3.5**).

In order to demonstrate if the cluster in MUV-10 might be compatible with the incorporation of other transition metal ions to access chemical compositions not accessible by direct synthesis, we next attempted the same experiments
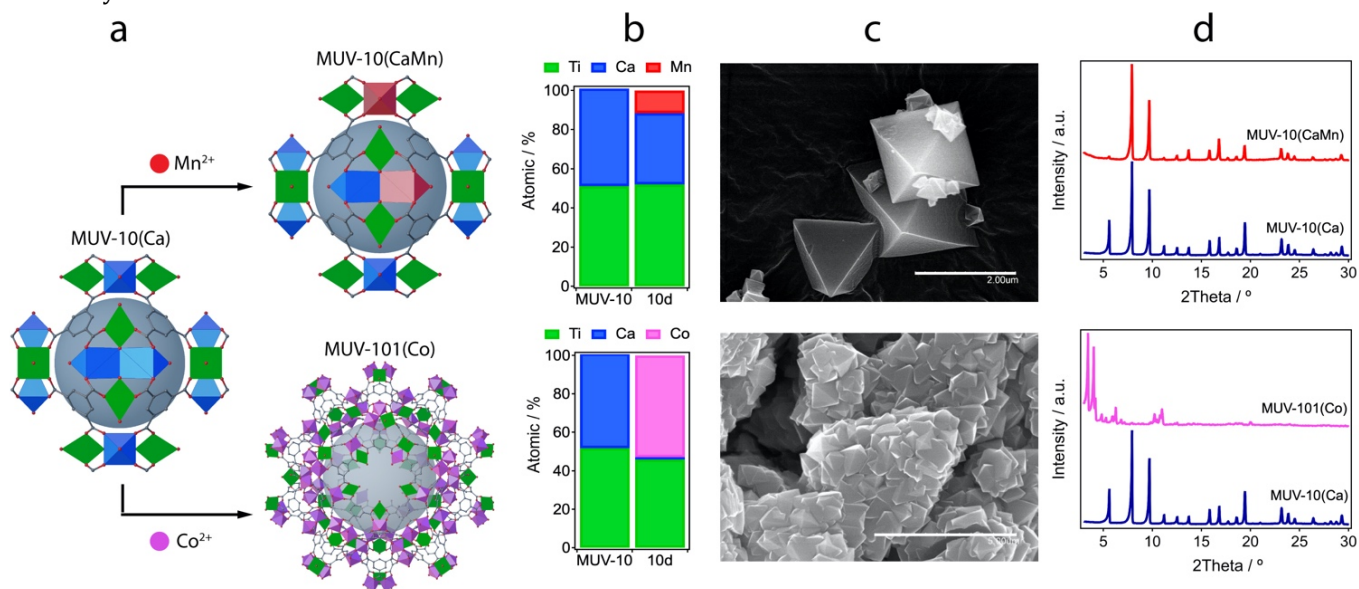


**Figure 2. Metal exchange reactions with MUV-10(Ca) crystals.** (a) Reaction of MUV-10(Ca) in methanolic solutions of $Mn^{2+}$ yields partial metal exchange with retention of the original structure whereas the same reaction with $Co^{2+}$ drives a topological transformation into MUV-101(Co). (b) Experimental metal replacement after 10 days, (c) SEM of the crystals and (d) PXRD after the experiment.

3

in presence of $Co^{2+}$. Soaking of MUV-10(Ca) in methanolic solutions of $Co(NO_3)_2 \cdot 6 H_2O$ (0.2M) at 65 °C resulted in the formation of a pink solid already after 10 days. Compared to partial replacement for the Mn case, the EDX analysis revealed that after this time metal exchange becomes quantitative for the case of Co with only slight traces of unexchanged calcium close to 0.1 % (**Figure 2b**, bottom). Quantitative metathesis has been reported for labile $[Cd_4O]^{6+}$ units[22] in MOF single crystals, but this drastic increase in substitution when moving from $Mn^{2+}$ to $Co^{2+}$ was unanticipated. To investigate its origin, we inspected the crystals with SEM after the reaction. Compared to transmetalation with Mn, that does not influence the original morphology, reaction with cobalt induces the formation of a cluster of micrometric crystals with octahedral morphology that completely occupy the original space of the seeding MUV-10(Ca) crystal (**Figure 2c**, bottom). EDX mapping of the crystals is again consistent with the formation of a single phase with a homogeneous distribution of Ti and Co throughout the newly formed crystals and complete depletion of Ca. However, PXRD reveals the complete transformation of the original material into a new phase that displays high crystallinity (**Figure 2d**, bottom). Rather than metal exchange, in the presence of $Co^{2+}$, MUV-10(Ca) seems to act as a templating scaffold that directs the growth of a new phase we will refer to as MUV-101(Co). In fact, PXRD Rietveld refinement of this newly formed phase confirmed that transmetalation induces a topological change for the formation of a heterometallic titanium-organic framework isostructural to MIL-100 (zeotipic *mtn* topology; **Supporting Section S4.4**).[13]

## Dynamic topological transformation of MUV-10 to MUV-101

We next investigated this phenomenon by isolating the crystals for different soaking times and analysing the transformation at the different stages (**Supporting Section S4**). SEM images reveal the formation of a corrugated surface on the facets of MUV-10(Ca) crystals after 12 hours of exposure to methanolic solutions of Co(II) (**Figure 3a**). This external layer directs the formation of small crystallization nuclei after 1 day, which evolve with time into micrometric crystals with octahedral morphologies that can be already visualised after 3 days. Newly formed crystals seem to keep growing continuously at expense of the original MOF to produce a cluster of intertwined crystals after 15 days, that keep the original size and shape of the MUV-10(Ca) templating scaffold. Overall, microscopic images suggest that both phases coexist and the formation of the MUV-101 phase proceeds by crystal-to-crystal transformation rather than crystallization from redissolution of MUV-10 in the reaction medium. This analysis was complemented with EDX measurements as function of the soaking time to account for the changes in chemical composition concomitant to the transformation of MUV-10 (**Supporting Section S4.2**). The data show a rapid incorporation of Co, that reaches a plateau at around 60 %

(at. %) after 15 days, parallel to the complete removal of calcium from the crystals. The relative titanium content decreases from 50 to 40 % until it stabilises for a relative Ti:Co ratio close to 1:2. Single point spectra of the chemical composition throughout the crystals is indicative of a homogeneous distribution of both metals in the expected ratio.

The study of the MUV-101 phase by single-crystal diffraction was not possible due to the intertwined nature of the crystals formed. Nevertheless, the structure was determined instead by refinement of high-resolution PXRD data collected by using synchrotron radiation (ALBA, BL04-MSPD) and using the structure reported for MIL-100(Ti) as starting model (CCDC 1871195).[27] Rietveld refinement converged with excellent residual values (Rwp = 3.95 %, Rexp= 1.77 %) to a cubic *Fd-3m* space group with cell parameters $a$ = 73.5784(8) Å (**Supporting Section S4.4**). MUV-101(Co) is isostructural to the prototypical MIL-100 family. Accordingly, heterometallic 6-c $TiCo_2$-SBUs are connected to six 3-c btc linkers to produce a zeolitic framework with mnt topology, that combines two types of mesoporous cages of 2.2 and 2.9 nm interconnected in the three dimensions. Whereas, in MIL-100 phases, the introduction of $M^{+3}$ (Cr, Fe, Al)[13,28,29] or $M^{+4}$ (Ti)[27] metals into the homometallic SBU $[M_3(\mu_3\text{-}O)(X)(H_2O)_2(RCO_2)_6]$ is counterbalanced by the coordination of different capping linkers (X = $F^-$, $Cl^-$, $OH^-$, $O^{2-}$) to the axial position of the metal positions for a neutral structure. In MUV-101(Co), the combination of $Co^{2+}$ and $Ti^{4+}$ drives the formation of $[TiCo_2(\mu_3\text{-}O)(H_2O)_3(RCO_2)_6]$ clusters with possibly only water molecules acting as terminal ligands. The metallic ratio fixed by this formula agrees well with the experimental value determined by EDX. Phase transformation was also evaluated by PXRD of the crystals at increasing soaking times. **Figure 3b** shows that the [2 2 0] and [3 1 1] low-theta diffraction lines characteristic of the MUV-101 phase, isostructural to MIL-100, are already intuited after only 12 hours and become clearly visible after 1 day. From that point, MUV-10 and MUV-101 phases coexist up to 5 days of reaction, when the reflections [1 1 0] and [1 1 1] characteristic of MUV-10 are not visible any longer. Rietveld refinements were used to calculate the relative phase percentages in these intermediate states. As shown in **Supporting Section S4.6**, the formation of MUV-101(Co) increases at expense of MUV-10(Ca) for relative percentages of 3, 11, 65 and 98 % after 1, 3, 10 and 30 days, respectively.

The gradual conversion of the $Ti_2Ca_2$ cluster in MUV-10 into $TiCo_2$ in MUV-101(Co) is also correlated with changes to the thermal stability of the solid isolated at different reaction times. Thermogravimetric analyses (TGA; **Figure 3c**, **Supporting Section S4.7**) shows a progressive decrease in the decomposition temperature upon incorporation of cobalt from 500 °C for MUV-10 down to a minimum of 440 °C in fully transformed MUV-101(Co) after 30 days. We argue that this is possibly due to the dilution on the relative
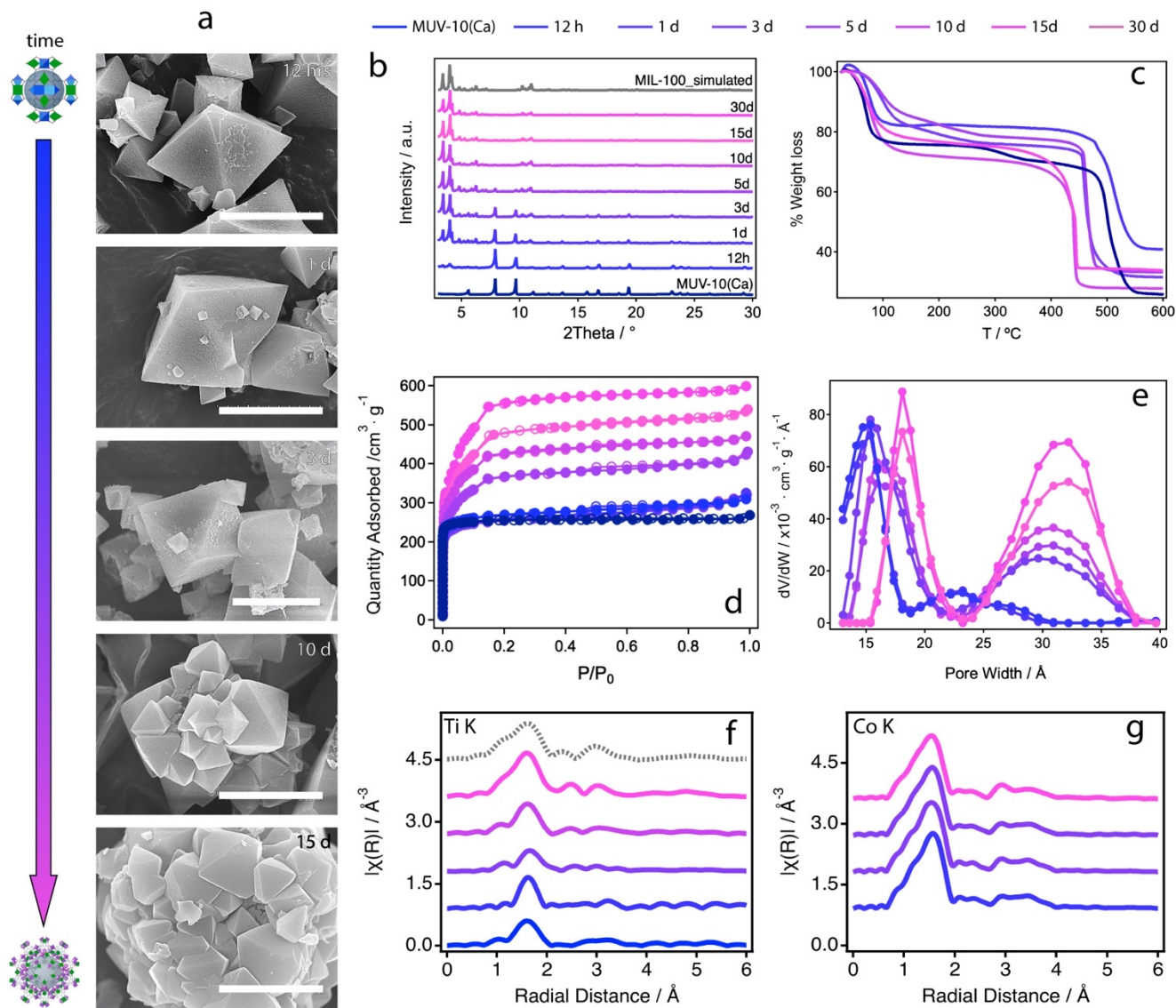
**Figure 3. Dynamic topological transformation of MUV-10(Ca) to MUV-101(Co).** (a) SEM images showing the progressive transformation of the crystals with time. Scale bars: 3μm. Analysis of the transformation at different reaction times: (b) PXRDs showing the transformation of MUV-10(Ca) into MUV-101(Co) with time; (c) Change in the chemical stability of the final material as result of the dilution of Ti-O bonds in TiCo₂ compared to Ti₂Ca₂ SBUs; (d) N₂ adsorption/desorption isotherms at 77 K showing the progressive increase in surface area with time; (e) Pore Size Distribution (PSD) showing the evolution in pore size until the formation of a mesoporous framework and (f, g) EXAFS Ti and Co-K edges spectra of MUV-101(Co) at different stages of transformation. The spectrum of MIL-100(Ti) was used for comparison and is showed as a dashed grey line. For a clearer analysis of the different stages of transformation see **Supporting Section S4.**

percentage of robust Ti-O bonds in the metal-oxo clusters, that decrease from 45 % in MUV-10(Ca) to 33 % in MUV-101. Nonetheless, the thermal stability of MUV-101(Co) is significantly higher than other homometallic phases as $Fe^{3+}$ and $Cr^{3+}$ which decompose between 300-350 °C.[13,28] We next collected standard N₂ isotherms for all the solids to investigate the effect of phase transformation in their porosity (**Figure 3d** and **Supporting Section S4.8**). All solids display a type I isotherm with increasing gas uptakes for higher degrees of transformation. Reaction time gradually increases multi-point BET surface area and pore volume values from 1054 m²·g⁻¹ and 0.47 cm³·g⁻¹ for MUV-101(Co)-12h, almost identical to the

MUV-10(Ca) phase, to almost the double for MUV-101(Co)-30d with 2043 m²·g⁻¹ and 0.92 cm³·g⁻¹. This value is consistent with the values reported for MIL-100 phases and confirms complete MOF-to-MOF conversion. The effect of this dynamic transformation over porosity can be more easily visualised by looking into the pore size distribution (PSD). As shown in **Figure 3e**, at short reaction times between 12 hours and 1 day PSD is dominated by a broad distribution of micropores centered at 1.5 nm and incipient mesoporosity between 2-3 nm. This intermediate stage is reminiscent of MUV-10(Ca) with an incipient formation of MUV-101(Co) and agrees well with the coexistence of both phases anticipated by Rietveld

5

analyses. The onset of mesoporosity is also consistent with the opening of a small hysteresis loop in the $N_2$ isotherm of these samples between $P/P_0$ = 0.4-1.0 (**Figure Supporting S45**). From 3 days and onwards the PSD reveals the formation of a mesoporous material with two pore sizes. The smaller one increases from up to 1.5 to 1.8 nm whereas the biggest one lies close to 3.2 nm, consistent with the prevalence of the MUV-101 phase at these stages. Overall, the sorption data suggest that this topological transformation might be useful to gain dynamic control over the formation of hierarchical micro/mesopore structures at intermediate stages of transformation. We also confirmed that the stability of the final material towards water degradation was not compromised by running stability tests by soaking MUV-101(Co)-30d crystals in acid, neutral and basic aqueous solutions (**Supporting Section S4.9**).

One of the main limitations in the synthesis of mixed-metal frameworks, either by direct or post-synthetic methods, is the likeliness of producing segregated single component phases rather than a homogeneous distribution of the metals at an atomic level in the structure of the heterometallic MOF.[18] This problem is generally not amenable to the characterization techniques used and requires more advanced tools as X-Ray absorption or high-resolution spectroscopies.[21] We used EXAFS (Ti and Co K-edges) to correlate the degree of transformation with the changes to the local composition and structure of the SBUs with time (**Figure 3f, g** and **Supporting Section S4.10**). Ti and Co $K$-edge EXAFS data collected on the MUV-101 phase at 77K demonstrate the presence of hetero-bimetallic $TiCo_2$ clusters, with Ti-Co distances of *ca.* 2.94 Å (**Supporting Table S7**). This intermetallic distance in the heterometallic cluster of MUV-101 is significantly shorter than the Ti–Ti distances seen in homometallic MIL-100(Ti) (*i.e.* 3.47 Å)[27] and agrees well with our DFT models and the crystallographic data reported for other heterometallic $TiCo_2$ clusters,[30] ruling out the formation of segregated phases. The detailed analyses of the Ti $K$-edge XANES region indicate the presence of a 3-component pre-edge feature at 4971.5 eV after long transmetalation times, characteristic of centrosymmetric 6-coordinated $Ti^{+4}$ centers.[31,32] The intermediate stages of transformation show more distorted octahedral geometries. Regarding the local structure of the cobalt centres in MUV-101(Co), Co $K$-edge XANES data show the presence of a pre-edge feature at 7709.2 eV after equivalent reaction times indicative of $Co^{2+}$ with slightly distorted octahedral geometries, consistent with the formation of $TiCo_2$ clusters.[33] For a better understanding of the transformation process at the nanoscale, we next used scanning transmission electron microscopy (STEM) with EDX to collect high-resolution elemental maps throughout a slice of the crystals (**Figure 4**). MUV-101(Co)-1d and 30d crystals were isolated, washed thoroughly and sectioned with focused ion beam (FIB). STEM-EDX of the lamellae at an early stage of transformation confirm that the material grown on the external surface of the crystal is richer in cobalt and poorer in calcium compared to the interior. This spatial control over chemical composition agrees well with a diffusion-controlled process in which metal exchange induces the formation of MUV-101(Co) at expense of MUV-10(Ca) crystals. We do not observe any signatures that

account for the deposition of amorphous oxide coatings or segregation of phases confirming the homogeneity of the process also at the nanoscale. Moreover, STEM-EDX spectral maps at different regions inside several crystals confirm the formation of a new material upon metal exchange with relative Ti, Co and Ca contents consistent with the EDX analyses of bulk crystals (**Supporting Section S4.11**).
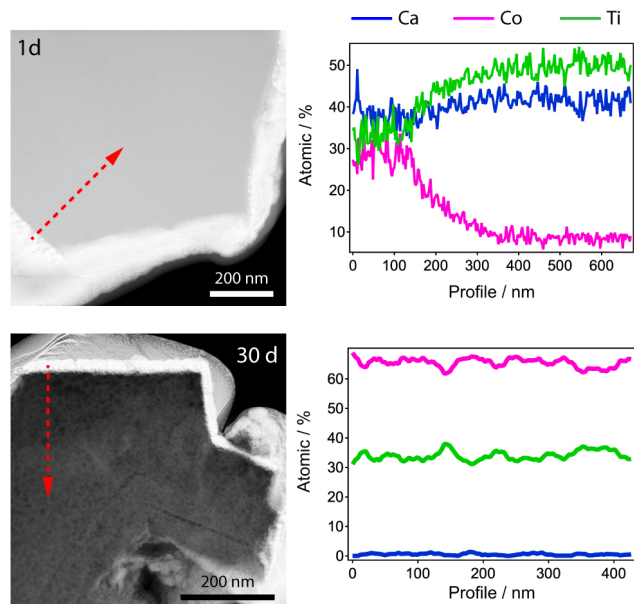


**Figure 4.** STEM-EDX of FIB-sectioned lamellae of MUV-101(Co)-1d and 30d showing the relative distribution of Ca (blue), Co (pink) and Ti (green) from the external surface to the inside of the crystal.

## Origin of the topological transformation

To put our results in context, we looked into the literature for other examples of MOF transformations by metal exchange reactions. Zhang and co-workers recently reported the transformation of HKUST into MIL-100. In this case, the poor stability of HKUST in the reaction medium induces the decomposition and redissolution of the crystals by hydrolysis in presence of $Fe^{3+}$, that is concomitant to the growth of nanoparticles of MIL-100(Fe).[34] In our case, the MOF transformation proceeds by crystal-to-crystal transformation from a chemically stable precursor.[24] The epitaxial growth of MOFs first reported by Kitagawa and co-workers,[35] involves the exposure to metal solutions of MOF crystals with surfaces that are end-capped by linkers capable to coordinate the incoming metal. As result, the outer surface of the crystal seeds the growth of an isostructural shell that is hybridized with the original core into a single mixed-metal crystal provided there is an excellent match between both lattices. In our case, the crystals of MUV-10(Ca) (***the***; cubic, Pm-3, a = 15.8362(8) Å) act as a templating scaffold and directs a topological transformation into MUV-101 (***mtn***; cubic, Fd-3m, a = 73.5784(8) Å). Compared to epitaxial growth, this process is driven by the generation of a new 6-c SBU resulting in the formation of a new topology compatible with the structural

6

information encoded in newly formed metal cluster and the 3-c organic linker common to both frameworks.

Intrigued by the differences with other MOF-to-MOF transformations available we decided to rationalize the origin of this phenomenon by analysing the surface terminations in MUV-10 crystals and studying the thermodynamics of the transformation of the SBU. We calculated the energies of (111), (001), and (110) surfaces representative of a cubic system with atomistic simulation techniques and used them to predict the equilibrium shape of the crystal through the Wulff construction method (see **Supporting Section S5** for computational methods).[36] As shown in **Figure 5b**, our results predict the formation of truncated octahedral crystals with preferential formation of (111) facets and small contributions from (001), with the last being responsible for truncation of the octahedral symmetry. The expression of (001) facets is not visible from SEM pictures, that show MUV-10 crystals with regular octahedral morphologies (**Figure 5a**). This deviation from our model is possibly due to the effect of the solvent or the modulator (acetic acid) over the crystallization of the MOF, which was not considered in our calculations and might disfavour the stabilization of (001) surfaces. Accordingly, metal exchange reactions in MUV-10 shall be dominated by the terminations of the dominant (111) surfaces. Cleavage of the crystal along this direction by using the GDIS package[37] reveals the coexistence of metal exposing (ligand free) and ligand capped terminations compatible with the

ligand or metal-exchange reactions required for structural transformation (**Figure 5c, d**). Similar terminations have been reported for other cubic MOFs as UiO or HKUST.[38,39] To confirm this point we performed additional metal exchange experiments with single crystals that reveal more clearly the nucleation of small seeds of MUV-101(Co) in the (111) facets of the octahedra (**Supporting Section S4.12**).

Our experimental results confirm the formation of heterometallic MUV-10(Mn) or MUV-101(Co) phases depending on the metal incorporated to the SBU. We hypothesized that MOF-to-MOF transformation might be ascribed to the instability of the heterometallic $Ti_2M_2$ cluster that is generated when $Ca^{2+}$ is replaced with $Co^{2+}$ rather than $Mn^{2+}$. Accordingly, we calculated the energy balance for the replacement of $Ca^{2+}$ nodes in $[Ti_2Ca_2(\mu_3-O)_2(H_2O)_4(RCO_2)_8]$ by these two metals. As shown in **Figure 5e**, the formation of an isostructural cluster is only thermodynamically favourable for $Mn^{2+}$ whereas it is disfavoured for $Co^{2+}$. These differences likely originate from the higher preference of Ca and Mn for a seven-fold CTP coordination environment compared to other first row transition metal ions as cobalt. We ascribe these differences to changes in the ionic radii, that decrease from 1.06 and 0.90 Å for $Ca^{2+}$ and $Mn^{2+}$ down to 0.65 Å for $Co^{2+}$.[40] Compared to $Co^{2+}$, the electronic preference of Mn for this coordination geometry agrees well with the structural trends extracted from the Cambridge Structural Database for heptacoordination across the transition metal series.[25]
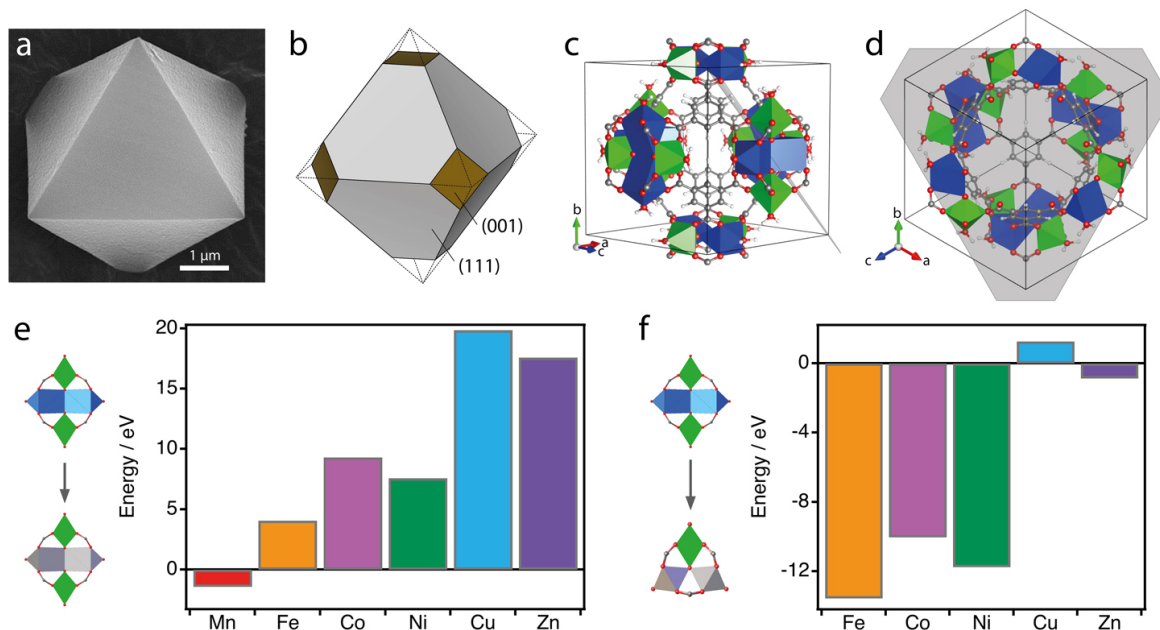


**Figure 5. Origin of the topological transformation.** (a) Experimental and (b) theoretical morphology of a crystal of MUV-10(Ca) calculated with the Wulff method. Differences are likely ascribed to the effect of the modulator used in the synthesis. (c) Perspective showing the cleavage of the cubic cell and the resulting (d) {111} surface termination combining metal and ligand free reactive sites. (e) Energy balance for the exchange of $Ca^{2+}$ sites in $[Ti_2Ca_2(\mu_3-O)_2(H_2O)_4(RCO_2)_8]$ ($Ti_2Ca_2$) SBUs with $Mn^{2+}$ (red), $Fe^{2+}$ (orange), $Co^{2+}$ (magenta), $Ni^{2+}$ (green), $Cu^{2+}$ (blue) and $Zn^{2+}$ (purple). Except for $Mn^{2+}$, metal-exchange would generate unstable coordination environments in isostructural clusters. (f) Enthalpy changes for the formation of $[TiM_2(\mu_3-O)(H_2O)_3(RCO_2)_6]$ ($TiM_2$) from $Ti_2Ca_2$ SBUs. Formation of $TiM_2$ metal-oxo clusters is disfavoured for $Cu^{2+}$ and thermodynamically possible for $Fe^{2+}$, $Co^{2+}$, $Ni^{2+}$ and $Zn^{2+}$ with a significant preference for the first three.

We argue this thermodynamic instability triggers the transformation of $Ti_2Co_2$ into more stable $TiCo_2$ SBUs. This was further confirmed by calculating the enthalpy for the formation of $[TiCo_2(\mu_3\text{-}O)(H_2O)_3(RCO_2)_6]$ from $[Ti_2Ca_2(\mu_3\text{-}O)_2(H_2O)_4(RCO_2)_8]$ clusters (**Figure 5f**), which indicates that the formation of the heterometallic $TiCo_2$ SBU is thermodynamically more favourable. Overall, this suggests that the transformation probably proceeds by metal exchange at the (111) surface of the crystal. Metal replacement would generate an offset in the coordination geometry of the $Ti_2Co_2$ heterometallic clusters that would evolve into the formation of more stable $TiCo_2$ SBUs. This would be the thermodynamic driving force guiding the formation of MUV-101(Co). Compared to the microporosity of MUV-10(Ca), the mesoporosity of MUV-101(Co) shall enable more favourable diffusion of mass for quantitative transformation from the outside to the inside of MUV-10(Ca) crystals.

gain more general understanding on the effect of the metal over the transformation phenomenon, we extended the calculations to other common divalent first row transition metal ions ($M^{+2}$ = Fe, Ni, Cu and Zn). Calcium exchange for the formation of heterometallic MUV-10(Ca) $Ti_2M_2$ clusters is also disfavoured for these metals following the order Cu > Zn >> Co > Ni > Fe with positive enthalpies of formation ranging from 19.9 to 4.1 eV for Cu and Fe, respectively (**Figure 5e**). These enthalpy changes are consistent with our previous periodic calculations for metal exchange in MUV-10(Ca).[24,25] In turn, the calculated formation enthalpies of $TiM_2$ from $Ti_2M_2$ display different trends depending on the metal identity (**Figure 5f**). Formation of $TiM_2$ SBUs is thermodynamically more favourable for Fe, Ni and Co, with energies ranging -13.6 to -10.0 eV, suggesting that these heterometallic phases of MUV-101 shall also be synthetically accessible. However, the small stabilization for the formation of $TiZn_2$ (-0.9 eV) suggests that this material might be difficult to produce under thermodynamic control. Finally, Cu is the only metal for which the formation of the heterometallic trimer is not energetically favourable. This is in line with the low crystal field stabilization energies expected for $Cu^{2+}$ and $Zn^{2+}$.[41] Provided the instability of $Ti_2Cu_2$ SBUs, our simulations suggests that exchange of MUV-10(Ca) crystals with copper might induce the formation of an alternative SBU for a different bipartite net compatible with the 3-c connectivity of btc linkers.

## Effect of the metal in directing the transformation

We performed additional metal exchange reactions to test the value of our theoretical predictions. MUV-10(Ca) crystals were soaked in concentrated solutions of Fe, Ni and Zn(II) nitrate salts using the same conditions described above (**Supporting Section S6**). As anticipated by our calculations, all metals display a similar behaviour and trigger the formation of coloured crystals that are visible after 10 days except for Zn. SEM-EDX and PXRD confirm the gradual exchange of $Ca^{2+}$, that becomes complete after 10 days for MUV-101(Zn) and 30 days for quantitative formation of crystals of MUV-101(Ni). MUV-101(Fe)-30d

shows close to 13 % of calcium indicative of an incomplete transformation, in good agreement with the presence of a residual fraction of the MUV-10 phase in the PXRD (**Figure Supporting S60**). This is possibly due to the difficulties in stabilizing $Fe^{2+}$ in solution for the long reaction times used in the experiment. $N_2$ isotherms of MUV-101(Ni)-30d and MUV-101(Zn)-10d are indicative of mesoporous solids with BET values and pore sizes consistent with the formation of highly crystalline heterometallic MIL-100 phases. MUV-101(Fe)-30d shows a significantly smaller surface area as result of the incomplete transformation. Overall, these results confirm the general value of MUV-10(Ca) as a precursor for inducing the formation of mesoporous, heterometallic titanium-organic frameworks by metal-exchange at low temperature. To check if these phases were kinetic in nature, we also attempted to produce MUV-101(Fe, Co, Ni, Zn) MOFs by direct synthesis at high temperature. Whereas MUV-101(Fe, Co, Ni) can be prepared by solvothermal reaction of titanium isopropoxide with the metal salts and btc in DMF,[42] MUV-101(Zn) can only be isolated by metal exchange reaction with MUV-10(Ca) at low temperature. These results agree well with our theoretical predictions that reveal a clear thermodynamic preference for the formation of $[TiM_2(\mu_3\text{-}O)(H_2O)_3(RCO_2)_6]$ SBUs for Fe, Co and Ni whereas Zn is significantly less favourable.[25] As result, this heterometallic phase can only be isolated by diffusion-controlled metal exchange rather than under thermodynamic control at high temperatures.

We next investigated the effect of $Cu^{2+}$ over the transformation. Our calculations above suggest that the formation of $TiCu_2$ clusters is not favourable so we expected significant differences in the product of the metal exchange reaction. For a clearer overview of the process, we analysed the progress of the reaction by isolating the product at different reaction times between 1 hour and 5 days (**Supporting Section S7**). SEM measurements confirms the formation of intertwined cubes at the facets of MUV-10(Ca) that become larger with time up to around 5 μm (**Figure 6a**). Compared to MUV-101(Co), reaction with $Cu^{2+}$ is roughly 3 times faster. The copper content reaches a plateau close to 80 % between 1 and 5 days, concomitant to the complete depletion of calcium from the crystals, for a final Ti:Cu ratio close to 1:4 (**Supporting Section S7.2**). These differences in the morphology of the crystals and relative metal ratio compared to MUV-101(Fe, Co, Ni, Zn), anticipated the formation of a different phase in the case of copper. This was first analysed with PXRD (**Figure 6b**), suggesting complete transformation after 1 day into a highly crystalline material that we will refer to as MUV-102(Cu). **Figure Supporting S80** shows the Le Bail refinement of the sample after 5 days confirming that the resulting material is isostructural to HKUST (***tbo***; cubic, Fm-3m, a = 26.343(5) Å). This MOF is built from the linking of 4-c paddlewheel $[Cu_2(CO_2)_2(H_2O)_2]$ SBUs and 3-c btc organic molecules. The total metal content corresponds to the incorporation of 20 % of titanium in MUV-102(Cu), suggesting the formation of one heterometallic TiCu clusters per 2.5 homometallic $Cu_2$ units. Just like with MUV-101(Fe, Co, Ni, Zn) or MIL-100(Ti), we argue that the excess
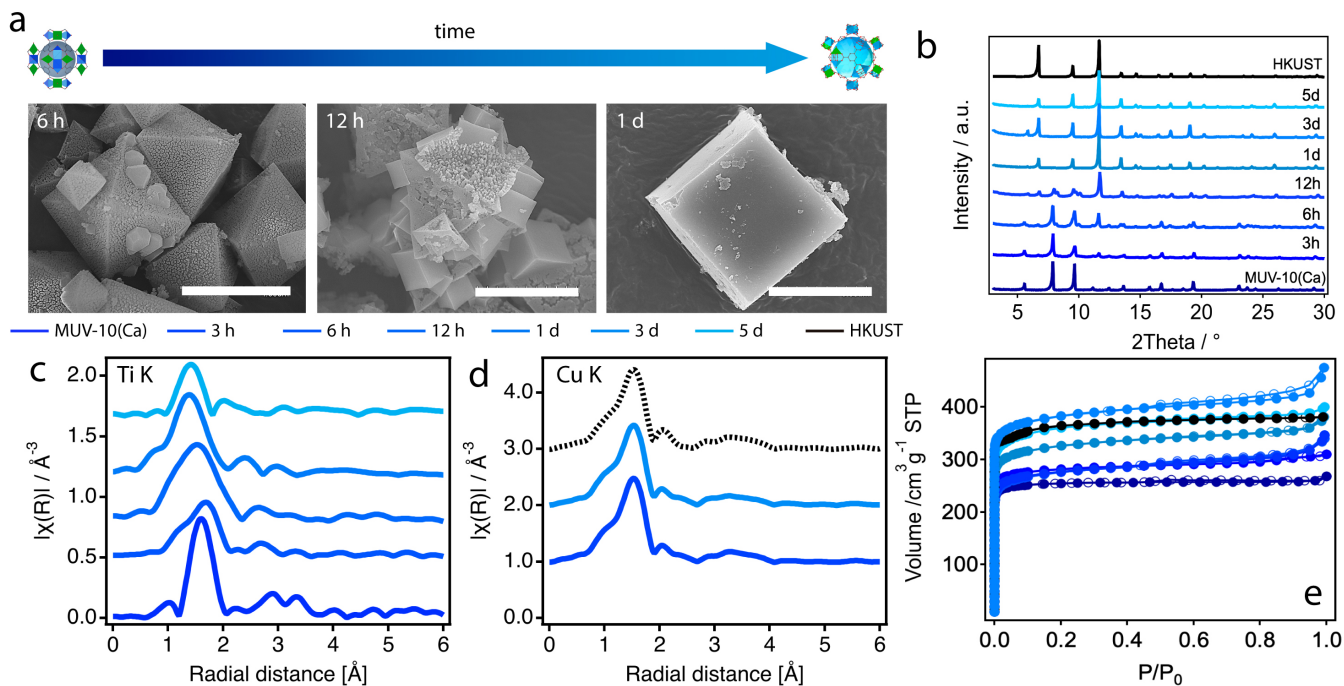
8

**Figure 6. Dynamic topological transformation of MUV-10(Ca) to MUV-102(Cu).** (a) SEM images showing the progress of the transformation with time for the formation of cube-like crystals of MUV-102(Cu). Scale bars: 3 μm. Analysis of the MOF transformation at different reaction times: (b) PXRDs showing the transformation of MUV-10(Ca) into MUV-102(Cu) with time and comparison with commercial HKUST (black); (c, d) EXAFS Ti and Cu-K edges spectra of MUV-102(Cu) at different stages of transformation. The spectrum of homometallic HKUST was used for comparison and is showed as a dashed black line; (e) $N_2$ adsorption/desorption isotherms at 77 K showing the progressive increase in surface area and pore volume with time until matching that of HKUST (black line). For a clearer analysis of the different stages of transformation see **Supporting Section S7.**

of positive charge that results from the replacement of $Cu^{+2}$ with $Ti^{+4}$ might be counterbalanced by the coordination of $O^{2-}$ capping linkers to titanium for a heterometallic $[TiCu_2(RCO_2)_2(O)(H_2O)]$ SBU. The formation of a heterometallic cluster agrees well with the evolution of the Ti *K*-edge EXAFS data with the reaction time (**Figure 6c,d**), which indicate the presence of Ti–Cu distances at *ca.* 2.84 Å for long reaction times in agreement with our DFT models for MUV-102(Cu) (**Supporting Table S15, Supporting Section S7.6**). Additionally, Ti and Cu *K*- edge XANES data demonstrated the simultaneous presence of highly distorted Ti(IV) 6-[31,32] and 5-coordinated Cu(II) centers[43,44] in MUV-102(Cu). We discarded the formation of nanometric thick oxide coatings upon transformation with STEM-EDX analyses. High-resolution spectral maps collected from FIB-sectioned crystals also confirm the formation of an outer shell of Cu that deepens into the crystal for increasing reaction times (**Supporting Section S7.7**). The formation of this binary *tbo* framework is consistent with $N_2$ gas sorption measurements. MUV-102(Cu) samples formed after transformations from 1 hour to 5 days display type-isotherms intrinsic to microporous materials with BET surface area vales and pore sizes increasing from 1000 m²·g⁻¹ and a micropore centered at 0.8 nm for MUV-102(Cu)-1h, characteristic of MUV-10, to 1509 m²·g⁻¹ and bimodal microporosity centered at 0.9 and 1.1 nm after complete transformation in MUV-102(Cu)-5d. We measured the porosity of a commercial sample of HKUST (Basolite® C300) soaked in MeOH for 5 days at room temperature to

confirm the excellent match in porosity between both samples (**Figure 6e and Supporting Section S7.8**). The low titanium doping does not affect notably the thermal and chemical stability of MUV-102(Cu) that displays a decomposition temperature of 302 °C and the same limitations toward water hydrolysis than homometallic HKUST (**Supporting Section S7.9 and S7.10**). Like with MUV-101(Zn), we could not prepare this heterometallic analogue of HKUST by direct synthesis confirming again the ability of metal-induced topological transformation to enable the formation of MOFs not accessible by *de novo* synthesis.

## Concluding remarks

The synthesis of titanium frameworks remains still limited by the difficulties in controlling the high reactivity of $Ti^{+4}$ ions in solution, that precludes the formation of persistent SBUs with the symmetry and connectivity required to target predefined topologies. We have shown the general value of MUV-10(Ca) as a precursor for directing the formation of mesoporous or microporous heterometallic titanium-organic frameworks at low temperature by exchange reactions with first row transition metals. Metal exchange at the soft positions of the cluster induces a MOF-to-MOF transformation that is controlled by the formation of thermodynamically favoured heterometallic clusters. As summarised in **Figure 7**, the nuclearity and nodes of connection of the resulting metal clusters is controlled by the metal incorporated and directs
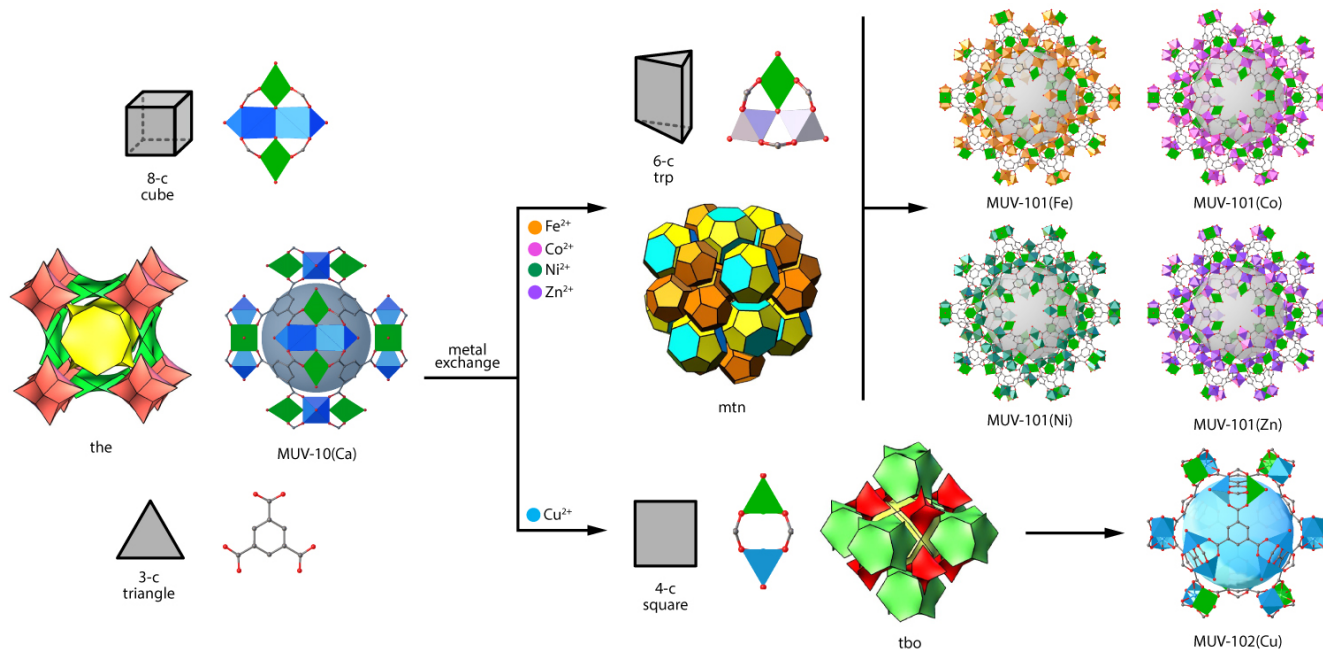
9

**Figure 7. Topological transformation chart.** Graphical overview of the binary heterometallic titanium-organic frameworks described in this work and their corresponding topologies and building units. Following the principles of reticular chemistry, the transformation of the 8-c $Ti_2Ca_2$ metal-oxo cluster in MUV-10(Ca) into 6-c $TiM_2$ and 4-c TiCu units by metal-exchange reaction drives the formation of the binary frameworks dictated by the local symmetries of 3-c btc units and the newly formed SBUs. All topologies shown have been taken from the Reticular Chemistry Structure Resource (RCSR; http://rcsr.anu.edu.au/).

the assembly of binary frameworks according to the principles of reticular chemistry. Compared to direct synthesis, this metal-induced topological transformation is a dynamic phenomenon and can be used to gain control over the formation of hierarchical micro/mesopore structures by controlling the extent of transformation with time for the synthesis of mixed phases. Our results also suggest that this method enables the formation of heterometallic titanium MOFs that are not accessible under solvothermal conditions at high temperature, thus opening the door for the synthesis multiple titanium heterometallic phases in the near future. Based on the advantageous properties of titanium and the intrinsic advantages of mixed-metal MOFs over their homometallic counterparts in applications as gas storage/separation or heterogeneous catalysis,[18,19] we are confident this approach might represent a turning point for the synthesis and general applications of titanium frameworks in a broad context.

## ASSOCIATED CONTENT

### Supporting Information

The Supporting Information is available free of charge on the ACS Publications website.

Synthetic and experimental details; physical characterization and supporting tables and figures (PDF)

X-ray crystallographic data for MUV-101(Co) (CIF)

## AUTHOR INFORMATION

### Corresponding Authors

*carlos.marti@uv.es
*nmpadial@scripps.edu

### ORCID

Natalia M. Padial: 0000-0001-6067-3360

Belen Lerma-Berlanga: 0000-0003-3686-8576

Neyvis Almora-Barrios: 0000-0001-5269-2705

Javier Castells-Gil: 0000-0001-7931-3867

Ivan Da Silva: 0000-0002-4472-9675

Ana E. Platero-Prats: 0000-0002-2248-2739

Sergio Tatay: 0000-0003-0785-866X

Carlos Martí-Gastaldo: 0000-0003-3203-0047

### Present Address

⊥ Department of Chemistry, Scripps Research, 10550 North Torrey Pines Road, La Jolla, CA 92037, United States.

### Author Contributions

# These authors contributed equally.

N.M.P. and C.M.-G. were responsible for the overall conception, direction and supervision of the project. N.M.P. and B.L.-B. performed most of the experimental work and data analysis. N.A.-B. was responsible for the computational work. J.C.-G. and I.dS. carried out the structural analysis. M.dlM., J.H.-S. and S.I.M. collected and analysed STEM data for high resolution elemental maps. J.H.-S. was responsible for sample preparation by FIB. S.T. and A.E.P.-P. were responsible for EXAFS data collection

10

and analysis. All authors discussed the results and contributed to the writing of the manuscript.

**Notes**

## ACKNOWLEDGMENT

## REFERENCES

1) Yaghi, O. M.; O'Keeffe, M.; Ockwig, N.; Chae, H.; Eddaoudi, M.; Kim, J. Reticular Synthesis and the Design of New Materials. *Nature* **2003**, *423*, 705-714.

2) Mason, J. A.; Oktawiec, J.; Taylor, M. K.; Hudson, M. R.; Rodriguez, J.; Bachman, J. E.; Gonzalez, M. I.; Cervellino, A.; Guagliardi, A.; Brown, C. M.; Llewellyn, P. L.; Masciocchi, N.; Long, J. R.Methane Storage in Flexible Metal–Organic Frameworks with Intrinsic Thermal Management. *Nature* **2015**, *527*, 357-361.

3) Tian, T.; Zeng, Z.; Vulpe, D.; Casco, M. E.; Divitini, G.; Midgley, P. A.; Silvestre-Albero, J.; Tan, J.-C.; Moghadam, P. Z.; Fairen-Jimenez, D. A Sol–Gel Monolithic Metal–Organic Framework with Enhanced Methane Uptake. *Nat Mater.* **2017**, *17*, 174-179.

4) Gu, C.; Hosono, N.; Zheng, J.-J.; Sato, Y.; Kusaka, S.; Sakaki, S.; Kitagawa, S. Design and Control of Gas Diffusion Process in a Nanoporous Soft Crystal. *Science* **2019**, *363*, 387–391.

5) Li, L.; Lin, R.-B.; Krishna, R.; Li, H.; Xiang, S.; Wu, H.; Li, J.; Zhou, W.; Chen, B. Ethane/Ethylene Separation in a Metal-Organic Framework with Iron-Peroxo Sites. *Science* **2018**, *362*, 443-446.

6) Cadiau, A.; Belmabkhout, Y.; Adil, K.; Bhatt, P. M.; Pillai, R. S.; Shkurenko, A.; Martineau-Corcos, C.; Maurin, G.; Eddaoudi, M. Hydrolytically Stable Fluorinated Metal-Organic Frameworks for Energy-Efficient Dehydration. *Science* **2017**, *356*, 731-735.

7) Diercks, C. S.; Liu, Y.; Cordova, K. E.; Yaghi, O. M. The Role of Reticular Chemistry in the Design of CO 2 Reduction Catalysts. *Nature Mater.* **2018**, *109*, 301-307.

8) Zhao, M.; Yuan, K.; Wang, Y.; Li, G.; Guo, J.; Gu, L.; Hu, W.; Zhao, H.; Tang, Z. Metal–Organic Frameworks as Selectivity Regulators for Hydrogenation Reactions. *Nature* **2016**, *539*, 76-80.

9) Eddaoudi, M.; Kim, J.; Rosi, N.; Vodak, D.; Wachter, J.; O'Keeffe, M.; Yaghi, O. M. Systematic Design of Pore Size and Functionality in Isoreticular MOFs and Their Application in Methane Storage. *Science* **2002**, *295*, 469–472.

10) O'Keeffe, M.; Yaghi, O. M. Deconstructing the Crystal Structures of Metal–Organic Frameworks and Related Materials into Their Underlying Nets. *Chem Rev* **2012**, *112*, 675-702.

11) Kalmutzki, M. J.; Hanikel, N.; Yaghi, O. M. Secondary Building Units as the Turning Point in the Development of the Reticular Chemistry of MOFs. *Sci. Adv.* **2018**, *4*, eaat9180.

12) Chui, S.; Lo, F.; Charmant, J.; Orpen, A. A Chemically Functionalizable Nanoporous Material $[Cu_3(TMA)_2 (H_2O)_3]_{(n)}$. *Science* **1999**, *283*, 1148-1150.

13) Ferey, G.; Serre, C.; Mellot-Draznieks, C.; Millange, F.; Surblé, S.; Dutour, J.; Margiolaki, I. A Hybrid Solid with Giant Pores Prepared by a Combination of Targeted Chemistry, Simulation, and Powder Diffraction. *Angew. Chem. Int. Ed.* **2004**, *43*, 6296-6301.

14) Férey, G.; Mellot-Draznieks, C.; Serre, C.; Millange, F.; Dutour, J.; Surblé, S.; Margiolaki, I. A Chromium Terephthalate-Based Solid with Unusually Large Pore Volumes and Surface Area. *Science* **2005**, *309*, 2040–2042.

15) Cavka, J.; Jakobsen, S.; Olsbye, U.; Guillou, N.; Lamberti, C.; Bordiga, S.; Lillerud, K. A New Zirconium Inorganic Building Brick Forming Metal Organic Frameworks with Exceptional Stability. *J. Am. Chem. Soc.* **2008**, *130*, 13850-13851.

16) Howarth, A. J.; Liu, Y.; Li, P.; Li, Z.; Wang, T. C.; Hupp, J. T.; Farha, O. K. Chemical, Thermal and Mechanical Stabilities of Metal-Organic Frameworks. *Nature Rev. Mater*. **2016**, *1*, 15018.

17) Furukawa, H.; Cordova, K. E.; O'Keeffe, M.; Yaghi, O. M. The Chemistry and Applications of Metal-Organic Frameworks. *Science* **2013**, *341*, 1230444.

18) Abednatanzi, S.; Derakhshandeh, P.; Depauw, H.; Coudert, F.-X.; Vrielinck, H.; Voort, P.; Leus, K. Mixed-Metal Metal–Organic Frameworks. *Chem. Soc. Rev.* **2019**, *48*, 2535-2565.

19) Masoomi, M.; Morsali, A.; Dhakshinamoorthy, A.; García, H. Mixed-Metal MOFs: Unique Opportunities in Metal-organic Framework Functionality and Design. *Angew. Chem. Int. Ed.* **2019**, *58*, 15188-15205

20) Santaclara, J. G.; Olivos-Suarez, A. I.; Nelson, A.; Osadchii, D.; Nasalevich, M. A.; van der Veen, M. A.; Kapteijn, F.; eveleva, A.; Veber, S. L.; Fedin, M. V.; Murray, A.T.; Hendon, C. H.; Walsh, A.; Gascon, J. Revisiting the Incorporation of Ti(IV) in UiO-Type Metal–Organic Frameworks: Metal Exchange versus Grafting and Their Implications on Photocatalysis. *Chem. Mater.* **2017**, *29*, 8963-8967.

21) Denny, M. S.; Parent, L. R.; Patterson, J. P.; Meena, S.; Pham, H.; Abellan, P.; Ramasse, Q. M.; Paesani, F.; Gianneschi, N. C.; Cohen, S. M. Transmission Electron Microscopy Reveals Deposition of Metal Oxide Coatings onto Metal–Organic Frameworks. *J. Am. Chem. Soc.* **2018**, *140*, 1348-1357.

22) Das, S.; Kim, H.; Kim, K. Metathesis in Single Crystal: Complete and Reversible Exchange of Metal Ions Constituting the Frameworks of Metal–Organic Frameworks. *J. Am. Chem. Soc.* **2009**, *131*, 3814–3815.

23) Brozek, C. K.; Dincă, M. $Ti^{3+}$, $V^{2+/3+}$, $Cr^{2+/3+}$, $Mn^{2+}$, and $Fe^{2+}$ Substituted MOF-5 and Redox Reactivity in Cr- and Fe-MOF-5. *J. Am. Chem. Soc.* **2013**, *135*, 12886-12891.

24) Castells-Gil, J.; Padial, N. M.; Almora-Barrios, N.; Albero, J.; Ruiz-Salvador, R. A.; González-Platas, J.; García, H.; Martí-Gastaldo, C. Chemical Engineering of Photoactivity in Heterometallic Titanium–Organic Frameworks by Metal Doping. *Angew. Chem. Int. Ed.* **2018**, *57*, 8453–8457.

25. Cremades, E.; Echeverría, J. & Alvarez, S. The trigonal prism in coordination chemistry. *Chem. Eur. J.* **2010**, *16*, 10380-10396.

26) Brozek, C. K.; Dincă, M. Thermodynamic Parameters of Cation Exchange in MOF-5 and MFU-4 L. *Chem. Commun.* **2015**, *51*, 11780–11782.

27) Castells-Gil, J.; Padial, N. M.; Almora-Barrios, N.; da Silva, I.; Mateo, D.; Albero, J.; García, H.; Martí-Gastaldo, C. De Novo Synthesis of Mesoporous Photoactive Titanium(IV)–Organic Frameworks with MIL-100 Topology. *Chem. Sci.* **2019**, *10*, 4313–4321.

28) Horcajada, P.; Surblé, S.; Serre, C.; Hong, D.-Y.; Seo, Y.-K.; Chang, J.-S.; Grenèche, J.-M.; Margiolaki, I.; Ferey, G. Synthesis and Catalytic

Properties of MIL-100(Fe), an Iron( Iii ) Carboxylate with Large Pores. *Chem. Commun.* **2007**, 2820 2822.

29) Volkringer, C.; Popov, D.; Loiseau, T.; Férey, G.; Burghammer, M.; Riekel, C.; Haouas, M.; Taulelle, F. Synthesis, Single-Crystal X-Ray Microdiffraction, and NMR Characterizations of the Giant Pore Metal-Organic Framework Aluminum Trimesate MIL-100. *Chem. Mater.* **2009**, *21*, 5695–5697.

30) Hong, K.; Bak, W.; Moon, D.; Chun, H. Bistable and Porous Metal–Organic Frameworks with Charge-Neutral AcsNet Based on Heterometallic $M_3O(CO_2)_6$ Building Blocks. *Cryst. Growth Des.* **2013**, *13*, 4066-4070.

31) Farges, F.; Brown, G. E. Coordination Chemistry of Titanium (IV) in Silicate Glasses and Melts: IV. XANES Studies of Synthetic and Natural Volcanic Glasses and Tektites at Ambient Temperature and Pressure. *Geochim. Cosmochim. Ac* **1997**, *61*, 1863–1870.

32) Henderson, G. S.; de Groot, F.; Moulton, B. X-Ray Absorption Near-Edge Structure (XANES) Spectroscopy. *Rev. Mineralogy Geochem.* **2014**, *78*, 75–138.

33) Hunault, M.; Vercamer, V.; Haverkort, M.; Arrio, M.-A.; Brouder, C.; Calas, G.; Juhin, A. Tracking the Signature of Low Symmetry Environments in the XAS K Pre-Edge. *J. Phys. Conf. Ser.* **2016**, *712*, 012005.

34) Li, W.; Zhang, Y.; Zhang, C.; Meng, Q.; Xu, Z.; Su, P.; Li, Q.; Shen, C.; Fan, Z.; Qin, L.; et al. Transformation of Metal-Organic Frameworks for Molecular Sieving Membranes. *Nature Commun.* **2016**, *7*, 11315.

35) Furukawa, S.; Hirai, K.; Nakagawa, K.; Takashima, Y.; Matsuda, R.; Tsuruoka, T.; Kondo, M.; Haruki, R.; Tanaka, D.; Sakamoto, H.; et al. Heterogeneously Hybridized Porous Coordination Polymer Crystals: Fabrication of Heterometallic Core–Shell Single Crystals with an In-Plane Rotational Epitaxial Relationship. *Angew. Chem. Int. Ed.* **2009**, *48*, 1766–1770.

36) Herring, C. Some Theorems on the Free Energies of Crystal Surfaces. *Phys. Rev.* **1951**, *82*, 87–93.

37) Fleming, S.; Rohl, A. GDIS: A Visualization Program for Molecular and Periodic Systems. *Zeitschrift Für Kristallographie – Cryst. Mater.* **2005**, *220*, 580–584.

38) Zhang, D.; Zhu, Y.; Liu, L.; Ying, X.; Hsiung, C.-E.; Sougrat, R.; Li, K.; Han, Y. Atomic-Resolution Transmission Electron Microscopy of Electron Beam–Sensitive Crystalline Materials. *Science* **2018**, *359*, 675-679.

39) Amirjalayer, S.; Tafipolsky, M.; Schmid, R. Surface Termination of the Metal-Organic Framework HKUST-1: A Theoretical Investigation. *J. Phys. Chem. Lett.* **2014**, *5*, 3206–3210.

40) Shannon, R. Revised Effective Ionic Radii and Systematic Studies of Interatomic Distances in Halides and Chalcogenides. *Acta Cryst.* **1976**, *32*, 751 767.
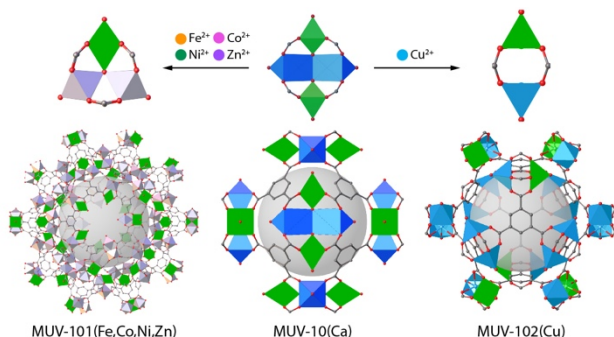
41) Cotton, A. F. I - Ligand Field Theory. *J. Chem. Educ.* **1964**, *41* (9), 466.

42) Castells-Gil, J.; M. Padial, N.; Almora-Barrios, N.; Gil-San-Millán, R.; Torres, V.; Romero-Ángel, M.; da Silva, I.; Waerenborgh, J. C.; Jagiello, J.; Tatay, S.; R. Navarro, J. A.; Martí-Gastaldo, C. Heterometallic Titanium-Organic Frameworks as Dual Metal Catalysts for Synergistic Non-Buffered Hydrolysis of Nerve Agent Simulants. *Submitted* (2020).

43) Todaro, M.; Sciortino, L.; Gelardi, F.; Buscarino, G. Determination of Geometry Arrangement of Copper Ions in HKUST-1 by XAFS During a Prolonged Exposure to Air. *J. Phys. Chem. C* **2017**, *121*, 24853–24860.

44) Borfecchia, E.; Maurelli, S.; Gianolio, D.; Groppo, E.; Chiesa, M.; Bonino, F.; Lamberti, C. Insights into Adsorption of NH 3 on HKUST-1 Metal–Organic Framework: A Multitechnique Approach. *J. Phys. Chem.* **2012**, *116*, 19839–19850.

## GRAPHICAL ABSTRACT



MUV-101(Fe,Co,Ni,Zn)      MUV-10(Ca)      MUV-102(Cu)

13